Characterization of the humanized FRG mouse model and development of an AAV-LK03 variant with improved liver lobular biodistribution

Marti Cabanes-Creus,[1] Renina Gale Navarro,[1] Sophia H.Y. Liao,[1] Suzanne Scott,[1] Rodrigo Carlessi,[2,3] Ramon Roca-Pinilla,[1] Maddison Knight,[1] Grober Baltazar,[1] Erhua Zhu,[4] Matthew Jones,[3] Elena Denisenko,[3] Alistair R.R. Forrest,[3] Ian E. Alexander,[4,5] Janina E.E. Tirnitz-Parker,[2,6] and Leszek Lisowski[1,7]

[1]Translational Vectorology Research Unit, Children's Medical Research Institute, Faculty of Medicine and Health, The University of Sydney, Westmead, NSW 2145, Australia; [2]Curtin Medical School, Curtin Health Innovation Research Institute, Curtin University, Bentley, WA 6102, Australia; [3]Harry Perkins Institute of Medical Research, QEII Medical Centre and Centre for Medical Research, The University of Western Australia, Nedlands, WA 6009, Australia; [4]Gene Therapy Research Unit, Children's Medical Research Institute and The Children's Hospital at Westmead, Faculty of Medicine and Health, The University of Sydney, and Sydney Children's Hospitals Network, Westmead, NSW 2145, Australia; [5]Discipline of Child and Adolescent Health, The University of Sydney, Sydney Medical School, Faculty of Medicine and Health, Westmead, NSW 2145, Australia; [6]UWA Centre for Medical Research, The University of Western Australia, Nedlands, WA 6009, Australia; [7]Laboratory of Molecular Oncology and Innovative Therapies, Military Institute of Medicine, 04-141 Warsaw, Poland

Recent clinical successes have intensified interest in using adeno-associated virus (AAV) vectors for therapeutic gene delivery. The liver is a key clinical target, given its critical physiological functions and involvement in a wide range of genetic diseases. In the present study, we first investigated the validity of a liver xenograft mouse model repopulated with primary hepatocytes using single-nucleus RNA sequencing (sn-RNA-seq) by studying the transcriptomic profile of human hepatocytes pre- and post-engraftment. Complementary immunofluorescence analyses performed in highly engrafted animals confirmed that the human hepatocytes organize and present appropriate patterns of zone-dependent enzyme expression in this model. Next, we tested a set of rationally designed HSPG de-targeted AAV-LK03 variants for relative transduction performance in human hepatocytes. We used immunofluorescence, next-generation sequencing, and single-nucleus transcriptomics data from highly engrafted FRG mice to demonstrate that the optimally HSPG de-targeted AAV-LK03 displayed a significantly improved lobular transduction profile in this model.

INTRODUCTION

Adeno-associated viruses (AAVs), from which the recombinant AAV (rAAV) vector system was derived, are putatively non-pathogenic parvoviruses endemic in the human population.[1] Wild-type AAV harbors a 4.7 kb single-stranded DNA genome encoding for non-structural (*rep*), structural (*cap*), assembly-activating (*aap*), and membrane-associated accessory (*maap*) proteins.[2,3] The three structural proteins, VP1, VP2, and VP3, assemble stochastically to form the capsid,[4] which determines the tropism of the virus and its reactivity with the immune system. Several features make AAV vectors desirable for clinical gene therapy applications, such as ease of large-scale manufacturability, low immunogenicity, and long-term expression in non-dividing cells.[5]

Since the capsid is the primary determinant of vector tropism, numerous strategies have been developed to bioengineer AAV capsids to create novel variants with improved tropism.[5] DNA-family shuffling is a strategy that involves the *in vitro* recombination of related parental genes which then encode recombinant VPs, giving rise to recombinant capsids.[6] In the context of DNA-family shuffling, capsid genes from multiple AAV variants or serotypes are randomly fragmented and subsequently reassembled based on partial homologies. These chimeric libraries are then screened for variants with desired properties, such as tissue specificity or the ability to evade the immune system.[7]

The focus of this work is understanding the liver lobular transduction profile of AAV-LK03,[8] a bioengineered AAV capsid selected in an *in vivo* screen of a shuffled capsid library in Fah$^{-/-}$/Rag2$^{-/-}$/Il2rg$^{-/-}$ (FRG)[9] chimeric mice repopulated with primary human hepatocytes. AAV-LK03 is currently being studied in several academic and commercial clinical programs, including a phase III clinical trial for hemophilia A.[10] While the *in vivo* selection and evaluation of AAV-LK03 served as critical proof of concept for the field of AAV capsid bioengineering, the selection was based on the ability to transduce primary human hepatocytes in the FRG xenograft model without considering the inherent structural complexity of the liver, which is heterogeneous
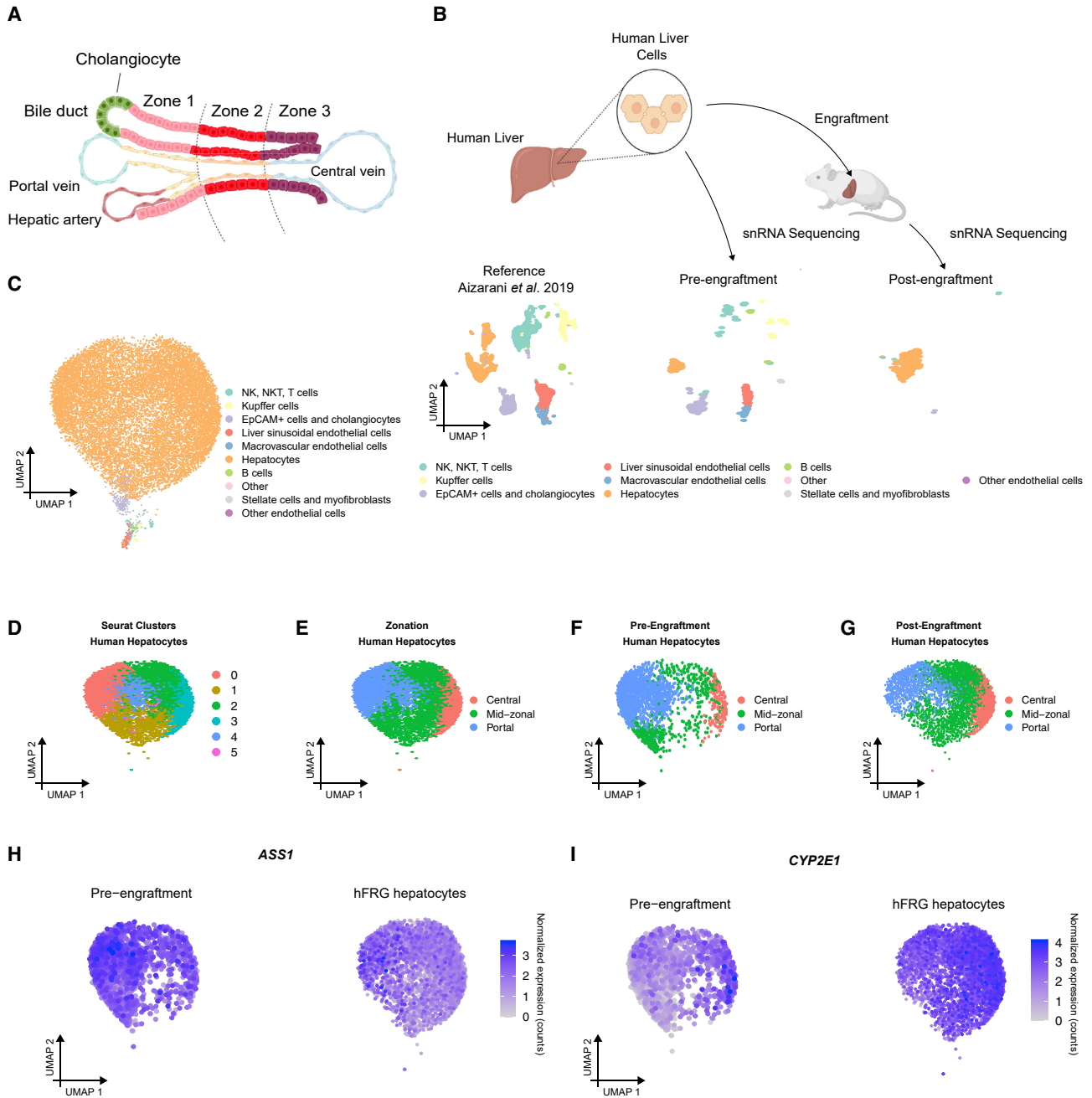
Figure 1. Characterization of human liver cells pre- and post-engraftment in the FRG mouse model with single-nucleus RNA sequencing

(A) Schematic representation of the liver lobule. Zone 1 is defined as the region closest to the portal triad, zone 2 spans in between zones 1 and 3, and zone 3 is located near the central vein. (B) Experimental design and UMAP visualization of single human hepatic nuclei. Liver cell types were annotated on the basis of integration with the Aizarani dataset.[13] (C) UMAP visualization of 7,309 single human hepatic nuclei with predicted cell types. (D) UMAP visualization of the unsupervised, graph-based clustering of the human hepatocyte population before and after engraftment in the FRG model. (E–G) Zonation mapping in the UMAP space of all human single-nucleus hepatocytes (E), the pre-engraftment sample (F), and the post-engraftment hepatocytes (G). (H and I) Log-normalized expression of ASS1 (periportal marker) and CYP2AE1 (pericentral marker) in the UMAP space on human nuclei analyzed before and after engraftment (humanized FRG hepatocytes).

on the level of morphometry and histochemistry.[11] This heterogeneity is related to the blood supply; consequently, hepatocytes are spatially heterogeneous along the portal-central axis of the liver lobule (Figure 1A).[12,13] The liver lobule has been divided into three metabolically distinct zones: the periportal zone surrounding the portal triad (portal vein, hepatic artery, and bile duct), the central zone nearest the

central vein, and the remaining mid-zone.[13] Since AAV vectors reach the liver with the blood from the portal triad, they first encounter hepatocytes in the periportal zone. We have recently reported a robust correlation between strong heparan sulfate proteoglycan (HSPG) binding affinity and periportal liver transduction in the murine liver for another bioengineered variant, AAV-KP1.[14] The phenomenon of zonal transduction was also observable for AAV8, a natural variant that presents a centrilobular profile in the murine liver,[15] when the introduction of mutations in the AAV8 capsid to increase HSPG binding resulted in a shift to marked periportal transduction.[16] AAV-LK03 inherited the capsid residues involved in HSPG binding from AAV3b, which shows a strong affinity for HSPG. Interestingly, just like AAV2, AAV3b was propagated *in vitro* before its capsid sequence was resolved,[17] and thus its strong HSPG binding could represent a tissue-culture adaptation rather than a characteristic of the naturally occurring serotype.[18] Recently, we demonstrated a marked increase in the liver lobule penetration and thus an increase of the lobule area amenable for vector transduction by reducing the HSPG-binding affinity of AAV-KP1, which, like AAV-LK03, also harbors the heparin-binding domain from AAV3b.[14]

The fact that in humanized FRG (hFRG) mice human hepatocytes proliferate in the scaffold of the mouse host liver and replace endogenous murine hepatocytes adds an extra layer of complexity when studying AAV-mediated liver lobule transduction. In this model, the process of liver repopulation by human hepatocytes is facilitated by a combination of genetically induced toxicity of endogenous murine hepatocytes and intrinsic immunodeficiency, as recently reviewed.[19] To date, assessment of xenograft models based on their ability to support the proper formation of hepatic zonation has largely remained elusive and controversial. For example, a study of the FRG system suggested that the humanized chimeric liver failed to form the hepatic zonation based on mathematical pharmacokinetic assessment.[20] In contrast, another study using uPA-SCID transgenic mice demonstrated that the chimeric liver of highly repopulated animals presented appropriate patterns of zone-dependent expression of representative cytochrome P450 (CYP) enzymes and arginase I.[21]

In the present study, we first investigated the validity of the xenograft FRG mouse model as a biologically predictive pre-clinical model of the human liver, using single-nucleus RNA sequencing (sn-RNA-seq)[22] to study the transcriptomic profile of primary human hepatocytes. Immunofluorescence analyses confirmed that in highly engrafted FRG animals the human hepatocytes organize and present appropriate patterns of zone-dependent enzyme expression.

Next, we tested a set of rationally designed HSPG de-targeted AAV-LK03 variants for relative transduction performance in highly engrafted FRG mice. We hypothesized that variants with decreased HSPG binding, and thus improved liver biodistribution in this model, should reach the human clusters with higher efficiency than parental AAV-LK03. Finally, we used immunofluorescence, next-generation sequencing (NGS), and single-nucleus transcriptomics data from highly engrafted FRG mice to demonstrate that the optimally HSPG de-targeted AAV-LK03 displayed a significantly improved lobular transduction profile. Such HSPG de-targeted vectors may carry the promise of therapeutic transgene delivery to all zones of the liver lobule, potentially putting all genetic disorders of the liver within therapeutic reach.

RESULTS

Human primary hepatocytes pre- and post-engraftment in xenograft mice maintain zonation markers but differ in zonal proportions

To study and characterize the transcriptomic profile of human hepatocytes before and after engraftment in the FRG xenograft model, we employed a droplet-based (10x Chromium) single-nucleus transcriptomics (sn-RNA-seq) approach, as described recently.[22] We isolated and profiled human hepatic nuclei from a 15-month-old female donor before (n = 2) and 6 months after liver engraftment in the FRG model, from flash-frozen ~25 mg of FRG liver chunks (n = 2). We obtained a total of 7,309 single human nucleus liver cell transcriptomes. To identify cell types, we integrated our dataset with the available human liver single-cell RNA sequencing (sc-RNA-seq) dataset published by Aizarani and colleagues (Figure 1B).[13,23] Although the commercial hepatocyte sample is enriched for human hepatocytes (>80%), this analysis revealed the presence of cell types expected to be present in the human liver (Table 1 and Figure 1B). Six months post engraftment, the vast majority (>99%) of the analyzed human transcriptomes originated from hepatocytes (Table 1 and Figure 1B).

Once we had identified the main cell types, we examined them using non-linear dimensionality reduction (uniform manifold approximation and projection [UMAP]). Figure 1C displays all the 7,309 single human liver nuclei with their cell-type identities. We subsequently focused on the human hepatocyte population. After integrating the datasets, a clustering analysis in Seurat identified six clusters (Figure 1D).

Hepatocytes have been described as having distinct functions based on their location in the hepatic acinus, known as hepatic or lobular zonation (Figure 1A).[24] The outer highly oxygenated periportal lobule layers express higher levels of enzymes involved in energy-demanding tasks such as gluconeogenesis and ureagenesis, whereas the inner pericentral layers specialize in glycolysis and xenobiotic metabolism.[24] Zone 1 (periportal) hepatocytes have a known role in gluconeogenesis and β-oxidation.[25] By studying the differential expression of genes on each identified cluster, we observed enriched expression of genes involved in lipid and cholesterol synthesis, such as *HMGCS1* and *ACSS2*, in cluster 4 (Figures 1D and S1), suggesting that this cluster may represent a subset of zone 1 hepatocytes.[26] Cluster 0 presented differential overexpression of genes involved in the urea cycle and histidine catabolism, such as *ASS1* and *HAL1* (Figures 1D and S1), also known as periportal markers. Thus, we also mapped cluster 0 to periportal (zone 1) hepatocytes.

In contrast, zone 3, or central venous, hepatocytes play a role in drug metabolism and detoxification, constitutively expressing high levels

Table 1. Single-nucleus count of the single human hepatic nuclei annotated on the basis of integration with the Aizarani dataset as described in Figure 1B

Cell type	Pre-engraftment #1		Pre-engraftment #2		Post-engraftment #1		Post-engraftment #2		Total	
	Count	Percentage	Count	Percentage	Count	Percentage	Count	Percentage	Count	Percentage
Hepatocytes	863	81.11	1,271	87.23	2,444	99.76	2,335	99.87	6,913	94.58
B cells	6	0.56	8	0.55	0	0.00	0	0.00	14	0.19
EPCAM+ cells and cholangiocytes	69	6.48	68	4.67	2	0.08	0	0.00	139	1.90
Liver sinusoidal endothelial cells	67	6.30	35	2.40	0	0.00	0	0.00	102	1.40
NK, NKT, T cells	33	3.10	34	2.33	4	0.16	3	0.13	74	1.01
Stellate cells and myofibroblasts	6	0.56	3	0.21	0	0.00	0	0.00	9	0.12
Kupffer cells	9	0.85	31	2.13	0	0.00	0	0.00	40	0.55
Macrovascular endothelial cells	11	1.03	7	0.48	0	0.00	0	0.00	18	0.25
Total	1,064		1,457		2,450		2,338		7,309	

Nuclei were analyzed before engraftment (n = 2) and in two independent mice (post-engraftment, n = 2).

of cytochrome P450 enzymes. Classic examples of zone 3 highly expressed liver genes with a pericentral pattern are *GLUL* and *CYP2E1*,[27] which would suggest that central and mid-zonal/central hepatocytes may be represented by cluster 3 in our analysis (Figures 1D and S1). Figure 1E summarizes the identified zonation identities of all the analyzed human hepatocyte nuclei before and after engraftment, and all the differentially expressed genes between the zones on both populations can be found in Table S1.

Overall, compared with the pre-engraftment hepatocytes, we found a higher proportion of human hepatocytes with mid-zonal/central characteristics in the post-engraftment sample (Figures 1F and 1G). We performed the analyses on nuclei extracted from frozen sections, which have been shown to have minimal bias based on cell survival.[28,29] This suggests that, at least in the hFRG model, either there is a selective expansion of zone 2/3 hepatocytes during the repopulation of the murine liver scaffold or there is a transition of zone 1 hepatocytes in the transcriptomic profile of the engrafted hepatocytes to support zone 2/3 functions. To distinguish between these two possibilities, we examined the expression of markers of liver regeneration. Although the role of pericentral AXIN2+ and LGR5+ hepatocytes in liver homeostasis and regeneration remains controversial,[30] we found *AXIN2* and *LGR5* to be significantly more expressed in the engrafted hepatocytes (Figures S2 and S3).

When comparing the pre-engraftment and post-engraftment portal hepatocytes, portal marker genes had significantly higher expression in the pre-engraftment condition, as exemplified with *ASS1* (Figure 1H; log fold change = 1.89, $p = 2.9 \times 10^{-234}$). Other known portal markers also presented similar differential superior expression in the pre-engrafted hepatocytes: *ASL1*: log fold change = 2.77, $p \approx 0$; *ARG1*: log fold change = 0.98, $p = 2.8 \times 10^{-177}$; *ACSS*: log fold change = 1.3, $p = 6.6 \times 10^{-107}$; and *HMGCS1*: log fold change = 0.75, $p = 6.9 \times 10^{-41}$.

In contrast to the periportal markers, we found a higher proportion of cells showing markers of pericentral hepatocytes in samples that had

been expanding in the hFRG for 6 months, as exemplified by *CYP2E1* (Figure 1I) and other pericentral markers such as the aforementioned *GLUL* (Figure S4). When it comes to the expression of human genes that have been linked to playing a role in AAV transduction, we found *KIAA0319L* (the gene encoding for the AAV receptor or AAVR[31]) to be widely expressed in most human hepatocytes before and after engraftment in hFRG (Figure S5).

The progeny of each individual engrafted hepatocyte can contribute to multiple metabolic zones

To complement the characterization of zonal populations in the hFRG with immunofluorescence, we studied the expression profile of four zonation markers in a highly engrafted hFRG (8.5 months post engraftment; human albumin at 12.34 mg/mL blood). We co-stained liver sections with human glyceraldehyde 3-phosphate dehydrogenase (hGAPDH) to mark human hepatocytes, and then either histidine ammonia-lyase (HAL), argininosuccinate synthetase (ASS), argininosuccinate lyase (ASL), or carbamoyl-phosphate synthase (CPS1) as portal markers and glutamine synthetase (GS) as a central marker (Figure 2A). In all four cases, we found clear signals of metabolic zonation, supporting the hypothesis that, at least in highly engrafted FRG mice, human hepatocytes organize and present appropriate patterns of zone-dependent expression. To investigate the species origin of the bile ducts in hFRG, we also stained sections of the same liver with cytokeratin 7 (CK7), a marker of epithelial cells present in larger biliary ducts.[32] Interestingly, we found that a significant part of this epithelial tissue was also of human origin (Figure 2B). We identified a nucleus population differentially expressing CK7 (*KRT7*) prior to engraftment. However, only a minor fraction of the nuclei, integrated within the hepatocyte population, showed significant levels of CK7 expression post engraftment when analyzed with sn-RNA-seq (Figure S6).

We next investigated the cellular origin of the observed metabolic zonation and potential epithelial transdifferentiation of hepatocytes into biliary cells. A humanization above 90% would give rise to
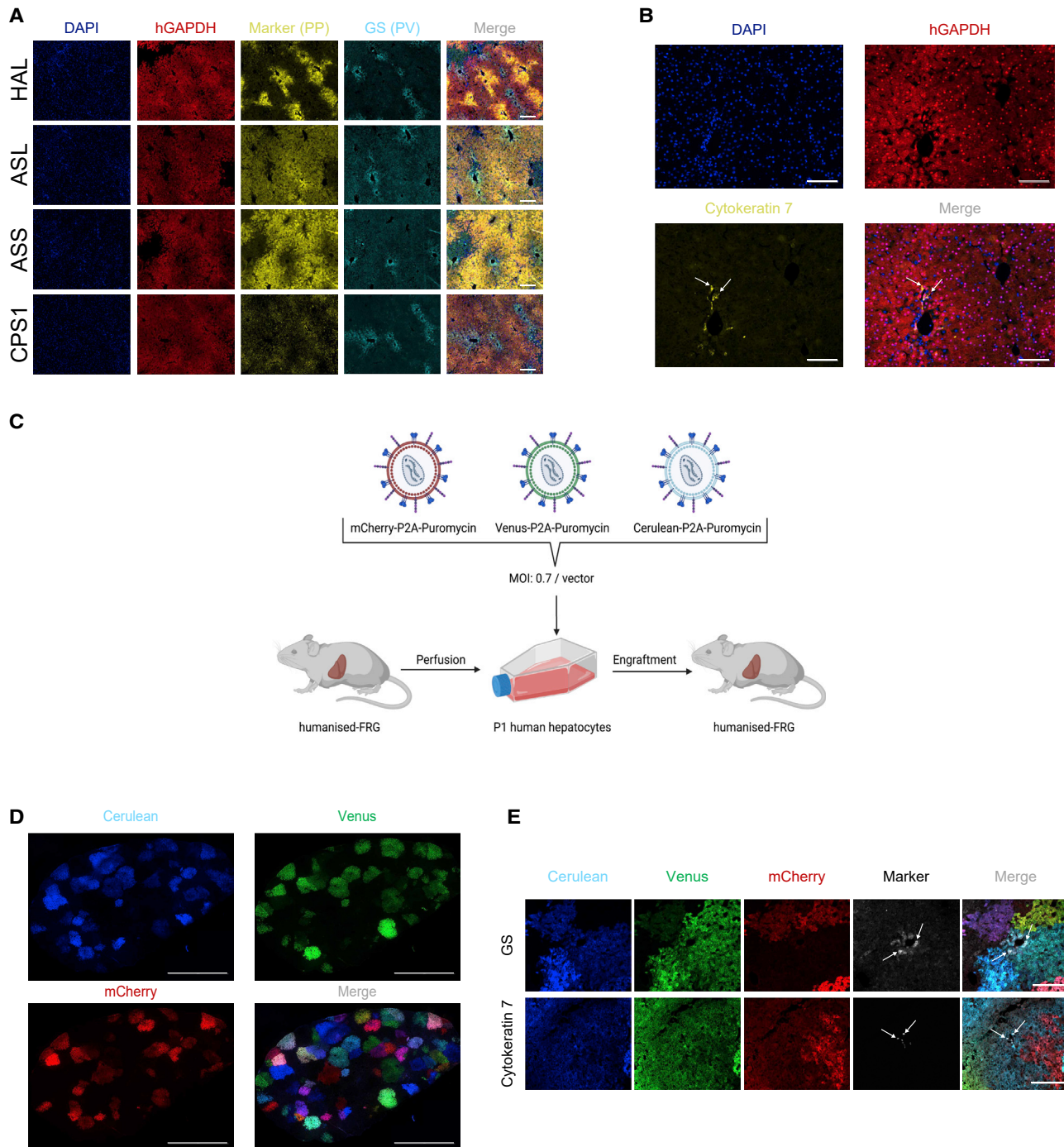
Figure 2. Immunofluorescence characterization of liver zonation in the FRG model

(A) Representative immunofluorescence analyses of a humanized FRG (hFRG) mouse liver stained with the indicated portal markers (yellow), the pericentral marker glutamine synthetase (GS, cyan), and human GAPDH (red), staining for human hepatocytes. HAL, histidine ammonia-lyase; ASL, argininosuccinate lyase; ASS, argininosuccinate synthetase; CPS1, carbamoyl-phosphate synthase; GAPDH, glyceraldehyde-3-phosphate dehydrogenase. Scale bars, 200 μm. (B) Representative immunofluorescence analysis of an hFRG mouse liver stained with human GAPDH (red) and cytokeratin 7 (yellow). Scale bars, 100 μm. (C) Schematic representation of the lentiviral transduction approach followed to genetically track human hepatocyte cluster origin in the hFRG model. (D) Representative immunofluorescence analysis of a hFRG mouse liver re-populated with human primary hepatocytes clonally transduced with lentiviral vectors encoding for Venus, Cerulean, and mCherry. Scale bars, 2,000 μm. (E) Immunofluorescence analysis of the hFRG presented in (D), co-stained with glutamine synthetase (top) and cytokeratin 7 (bottom). Scale bars, 200 μm.

around 120 million human hepatocytes per gram of liver mass (assuming 135 million hepatocytes per gram of liver mass[33]). Given that we routinely engraft 250,000 human hepatocytes per FRG animal, it seems plausible that hepatocytes from different pre-existing metabolic origins could adapt their transcriptomic profile depending on their spatial location during clonal expansion. To test this hypothesis, we took advantage of the previously reported multicolor panel of lentiviral "gene ontology" vectors,[34] which we modified to include a P2A-puromycin resistance downstream of the fluorophore (Figure 2C). In brief, we perfused a highly engrafted FRG mouse (>90% humanization), enriched the population to >95% human with magnetic bead/antibody purification, and plated these hepatocytes of mixed metabolic origin (termed P1 for murine passage 1) in collagen-coated plates. We subsequently co-transduced the hepatocytes with the three lentiviral constructs encoding Venus, Cerulean, and mCherry under the SFFV promoter at a multiplicity of transduction (MOT) of 0.7 per vector to bias the transduction toward one vector per cell. Next, we selected transduced cells with puromycin, and 1 week after transduction we harvested the individually transduced, and thus color-coded, hepatocytes, mixed them, and used them to engraft a naive FRG mouse. Finally, we harvested the chimeric liver 3 months after engraftment when the human albumin in the blood had reached 10.07 mg/mL, indicating >80% engraftment (Figure 2C). As shown in Figure 2D, when overlaying the three fluorophores each clonally expanded cluster presents a unique color identity, indicating that clusters originated from a single engrafted cell. In addition, we stained for the central marker GS and observed that only the cells surrounding the central vein were positive. However, hepatocytes from the same-colored cluster expanded beyond that area (Figure 2E). We observed the same phenomenon for the biliary marker CK7 (Figure 2E). These data support the hypothesis that engrafted hepatocytes have the capacity to transdifferentiate into cells of different metabolic zones as well as intrahepatic biliary epithelium.

Attenuation of HSPG binding increases the area amenable to AAV-LK03 transduction in hFRG mice

Historically, assessment of liver lobular transduction of human-tropic AAV vectors has proven difficult because of observed discrepancies between physical and functional transduction of human-tropic AAV variants in the murine liver when using single-stranded DNA transgenes.[14] Recently, we reported that the insertion of a single amino acid at capsid position 265 (265insT[14]) allowed for functional comparisons of human-tropic variants in the murine liver. AAV-LK03 harbors the heparin-binding motif of AAV3b,[35] and its murine surrogate (AAV-LK03_265insT) presented a marked periportal transduction profile.[14] We hypothesized that attenuating the binding affinity of AAV-LK03 to HSPG would allow for the generation of variants with improved lobular distribution and that this should translate into a superior targeting of human clusters in vivo (Figure 3A).

To test this, we rationally designed four AAV-LK03s to attenuate their affinity for HSPG. We generated two variants (AAV-LK03-R488Q and AAV-LK03-N583S) that, based on our previous studies on AAV2 HSPG binding,[16] were predicted to have decreased affinity

for HSPG. We also generated a variant where we substituted the critical arginine for HSPG binding[35] for glycine as in AAV3a[36] (AAV-LK03-R594G). Finally, we designed a variant where we incorporated two changes, D598H, which is also observed in AAV3a,[36] and R594E, with the intention to further reduce HSPG binding when compared with R594G. This last variant is referred to throughout this paper as AAV-LK03-REDH.[36] We tested the binding affinity of these four variants using a HiTrap Heparin Column. R488Q and N583S only slightly affected the elution profile, whereas substituting the critical R594 had a significant impact on the vector affinity to heparin (Table S2).[16]

To enable the simultaneous study of the parental AAV-LK03 control and the designed four variants in the same animal, we independently packaged five barcoded ssAAV-LSP1-GFP-BC-WPRE-BGHpA[16] expression cassettes per AAV variant. The barcodes allow for multiplexed high-throughput in vivo comparisons using NGS, as described in detail recently.[37] We injected the mix intravenously (5×10^{10} vector genomes [vg] per variant) into two hFRG mice with an average replacement index (RI)[19] of 80% and studied their relative performance in primary human hepatocytes 1 week after injection. To do so, we perfused the chimeric livers and isolated human hepatocytes by fluorescence-activated cell sorting (FACS), extracted DNA from the sorted cells, and analyzed the transgene barcode composition by NGS. After normalizing the number of reads mapped to each barcode to the vector composition in the pre-injection mix, we identified the double mutant AAV-LK03-REDH (R594E + D598H) as a variant with a superior in vivo transduction in the hFRG model (Figures 3B and S7). We subsequently focused on studying the differential in vivo performance of AAV-LK03 and the AAV-LK03-REDH double mutant.

First, to be able to visually compare the two vectors in the same animal using immunohistochemical analysis, we developed a strategy, shown schematically in Figure 3C, which consists of a modification of a recently published murine liver perfusion protocol (see materials and methods). In brief, we cloned Venus[38] and Cerulean[39] fluorescent protein reporters under the control of the CAG promoter in a self-complementary AAV cassette described previously.[40] To be able to track the transgenes at the DNA and RNA levels, we included a unique 50-mer DNA barcode compatible with single-nucleus transcriptomics between the stop codon and the SV40 poly(A) (Figure 3C). After packaging each capsid with either transgene (Venus or Cerulean), we titered and mixed them at 1:1 ratio with the complementary transgene packaged in the other capsid (AAV-LK03-Venus + AAV-LK03-REDH-Cerulean and AAV-LK03-Cerulean + AAV-LK03-REDH-Venus) (Figure 3C).

To study the model presented in Figure 3A, we co-injected 1×10^{11} vg of either vector mix into two FRGs engrafted with human hepatocytes. At 1 week post injection, we surgically isolated the left lobe prior to perfusing the rest of the liver to obtain a single-cell solution amenable for FACS (Figure 3C). We sorted human and mouse cells following a recently reported protocol (materials and methods and
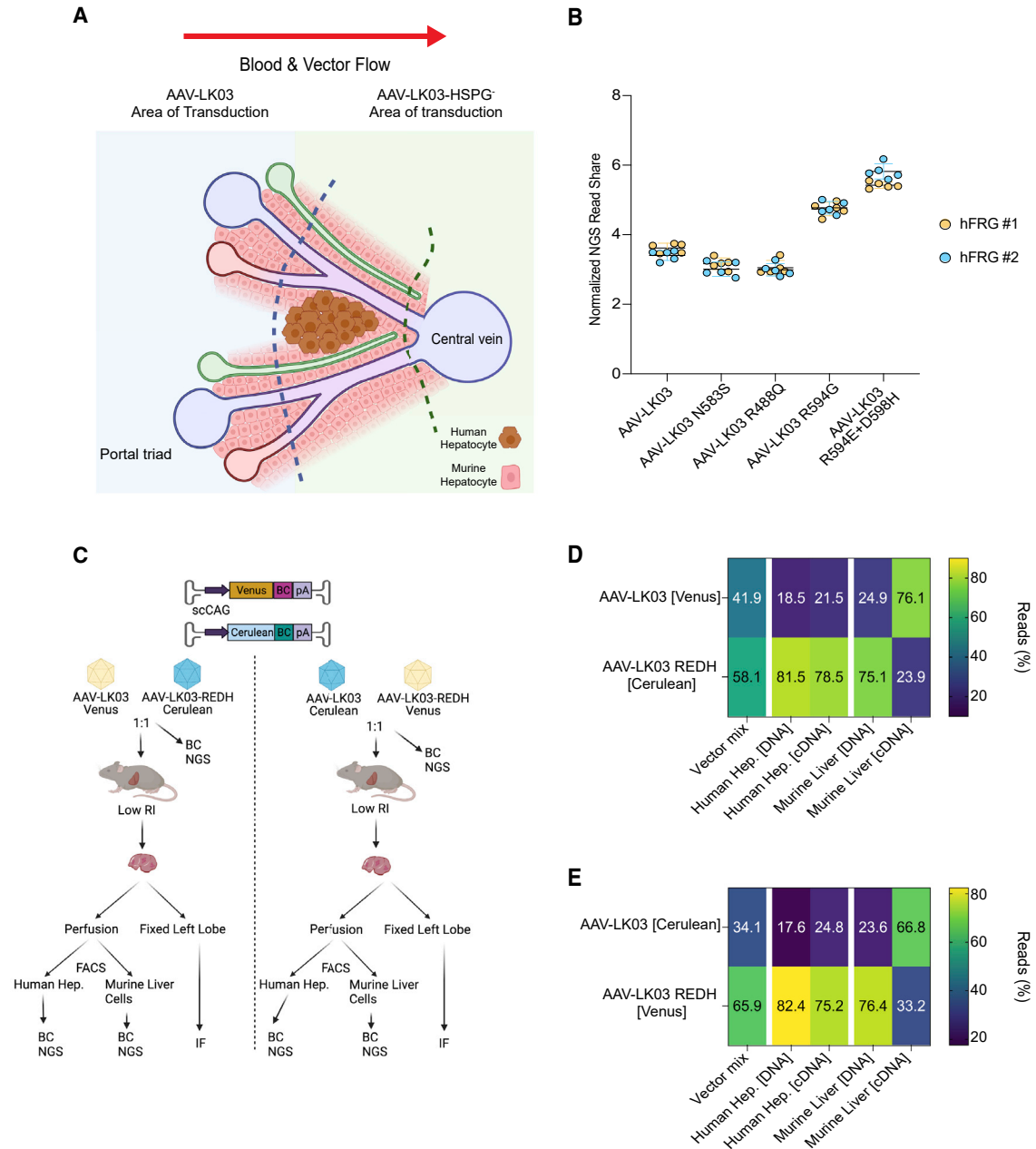
Figure 3. Identification of a novel HSPG de-targeted AAV-LK03 presenting an increased area of lobular transduction

(A) Schematic representation of the proposed transduction model for AAV-LK03 and the HSPG de-targeted AAV-LK03 variants in low-engrafted mice. Owing to high HSPG binding, the amenable area for transduction for AAV-LK03 is limited to the portal area (blue background). By reducing its interaction with this molecule, a wider lobular transduction might be achieved (green area). (B) *In vivo* comparison of AAV-LK03 and AAV-LK03 HSPG de-targeted variants based on physical transduction in the xenograft liver model (n = 2). Normalized percentage of NGS reads mapped to each capsid in human cells at the DNA level is shown. (C) Schematic representation of the study design comparing AAV-LK03 and AAV-LK03-REDH in low-engrafted mice. (D and E) *In vivo* comparison of AAV-LK03 and AAV-LK03-REDH in low-engrafted animals. Normalized percentage of NGS reads mapped to each capsid in human hepatocytes and murine liver cells at the DNA and cDNA are shown (n = 2). In (D), AAV-LK03 was encoded for Venus and AAV-LK03-REDH for Cerulean. The opposite mix was generated for (E).

Cabanes-Creus et al.[37]). We analyzed the relative vector performance at the levels of physical entry (DNA) and functional transduction (RNA/cDNA) in the human and murine cells using NGS

(Figures 3D and 3E). All reads were normalized to the pre-injection mixes to account for any variability in the composition of the initial mix (Table S3). As expected, the data from both sets of transgene

mixes showed that the vector performance was highly, if not wholly, dictated by the capsid serotype rather than by the transgene (Figures 3D and 3E). The double mutant AAV-LK03-REDH performed better than parental AAV-LK03 in the human hepatocytes present in low-engrafted hFRGs, both at the entry and functional levels (Figures 3D and 3E). However, we detected a loss in percentual potency at the functional transduction (RNA/cDNA) level when comparing the double mutant with AAV-LK03. This phenomenon was more evident when studying the performance of these two variants in the murine liver. Although we could detect a relatively larger number of reads associated with the double mutant AAV-LK03-REDH at the DNA level in the murine liver, the double mutant failed to express at the same level as AAV-LK03 and, thus, the overall mapped reads at the RNA/cDNA level were superior for AAV-LK03 (Figures 3D and 3E).

To complement the NGS data with immunofluorescence analyses, we fixed and stained the unperfused left lobe of the same animals with hGAPDH and GS to map human and murine pericentral hepatocytes.[27] As inferred from the NGS data, the double mutant AAV-LK03-REDH presented a superior transduction profile in low-repopulated (low RI) hFRG, with the expression of AAV-LK03-REDH-encoded Cerulean (Figures 4A and 4C) or Venus (Figures 4B and 4D) co-localizing mainly with the human clusters. On the other hand, AAV-LK03 expression was mainly reduced to the periportal area (Figures 4C and 4D). It is worth noting here that in striking contrast to the expression deficiency observed in single-stranded transgenes for AAV-LK03 in the murine liver[14] we detected Venus and Cerulean in portal hepatocytes of murine origin, suggesting that the previously postulated AAV-LK03 deficiency in the murine liver[14] may be driven by specific mechanisms occurring inside the target cell after entry but prior to single-stranded to double-stranded genome conversion.

AAV-LK03-REDH can penetrate deeper into the liver lobule than the parental AAV-LK03
Next, we studied the performance of both prototypical AAV-LK03 and the double mutant (AAV-LK03-REDH) in hFRG mice presenting a high level of human repopulation. As depictured schematically in Figure 5A, we hypothesized that since more human hepatocytes would be present within the periportal zone, which is amenable to AAV-LK03 transduction, the performance of AAV-LK03 would improve in highly repopulated animals when compared with animals with low RI.

We followed a similar approach to the previous experiment to study our hypothesis. Specifically, we injected an equimolar mix of vectors encoding Venus or Cerulean (AAV-LK03-Venus + AAV-LK03-REDH-Cerulean and AAV-LK03-Cerulean + AAV-LK03-REDH-Venus at 5×10^{11} vg/capsid) into two highly engrafted hFRGs (Figure 5B). In contrast to previous studies (Figure 3C), we also performed single-nucleus transcriptomics-based transduction analysis of the left lobes by taking advantage of the unique 50-mer DNA barcode placed immediately before the poly(A) (Figure 5B).

As shown in Figures 5C and 5D, AAV-LK03-REDH could still physically transduce a more significant proportion of the human hepatocytes (Figures 5C and 5D). Interestingly, AAV-LK03 displayed a more favorable DNA-to-RNA conversion as observed previously (Figures 3D and 3E), given that a relatively lower percentage of DNA reads for AAV-LK03 gave rise to a relatively higher percentage of cDNA reads. As discussed in more detail below, this phenomenon could be linked to either faster transduction kinetics for AAV-LK03 or to the existence of a "threshold effect," a minimal number of copies per cell required to yield successful functional transduction.

The immunofluorescence study of the liver sections from the same animals confirmed the trends observed with NGS (Figures 6A and 6B). Interestingly, and in agreement with our hypothesis regarding the influence of HSPG binding on zonal transduction, even at this high RI, AAV-LK03 functional transduction was still highly limited to portal hepatocytes even if those were of murine origin. In contrast, the HSPG de-targeted variant (AAV-LK03-REDH) functionally transduced human hepatocytes more efficiently than AAV-LK03. However, we observed higher transduction of human hepatocytes at the edges of the human clusters (Figures 6A and 6B).

Analysis of liver lobular AAV transduction with single-nucleus RNA sequencing
We next wanted to analyze the performance of each capsid with sn-RNA-seq. To do so, as discussed previously, we extracted and sorted nuclei from an unperfused snap-frozen fragment of the left lobe of the same highly engrafted hFRG animals[22] (Figure 5B).

Given the differential performance of both vectors in the murine cells at the cDNA (Figures 5C and 5D) and protein levels (Figures 6A and 6B), we extended the analysis to human and murine hepatocytes. We identified the cluster corresponding to murine hepatocytes with PanglaoDB. This web server allows for cell-type exploration and identification[41] (Figure 7A). The murine hepatocyte cluster was characterized by the expression of the murine genes *Alb*, *Cyp2e1*, and *Ttr* (Figure S8). The murine hepatocytes were particularly useful when validating the sn-RNA barcode strategy because based on the immunofluorescence results, we expected a clear difference between the expression of the barcoded transgene packaged in AAV-LK03 and the matching control transgene packaged in the HSPG de-targeted AAV-LK03-REDH (Figures 7A and 7B). Figure 7B displays human and murine clusters transduced with AAV-LK03-Cerulean, showing that we could obtain Cerulean transcripts in the murine hepatocytes to a larger extent than we could detect Venus transcripts (packaged in AAV-LK03-REDH). As expected, when we flipped the capsids and transgenes, we observed Venus expression mainly in murine hepatocytes and restricted Cerulean expression in those cells (Figure 7C).

Once we had validated the sn-RNA barcoded strategy, we focused our analysis on the transduction profile of each capsid variant in human hepatocytes (Figures 7D and 7E), with particular focus on their lobular transduction profile. As expected, based on the immunofluorescence results, a more significant proportion of portal and mid-zonal hepatocytes
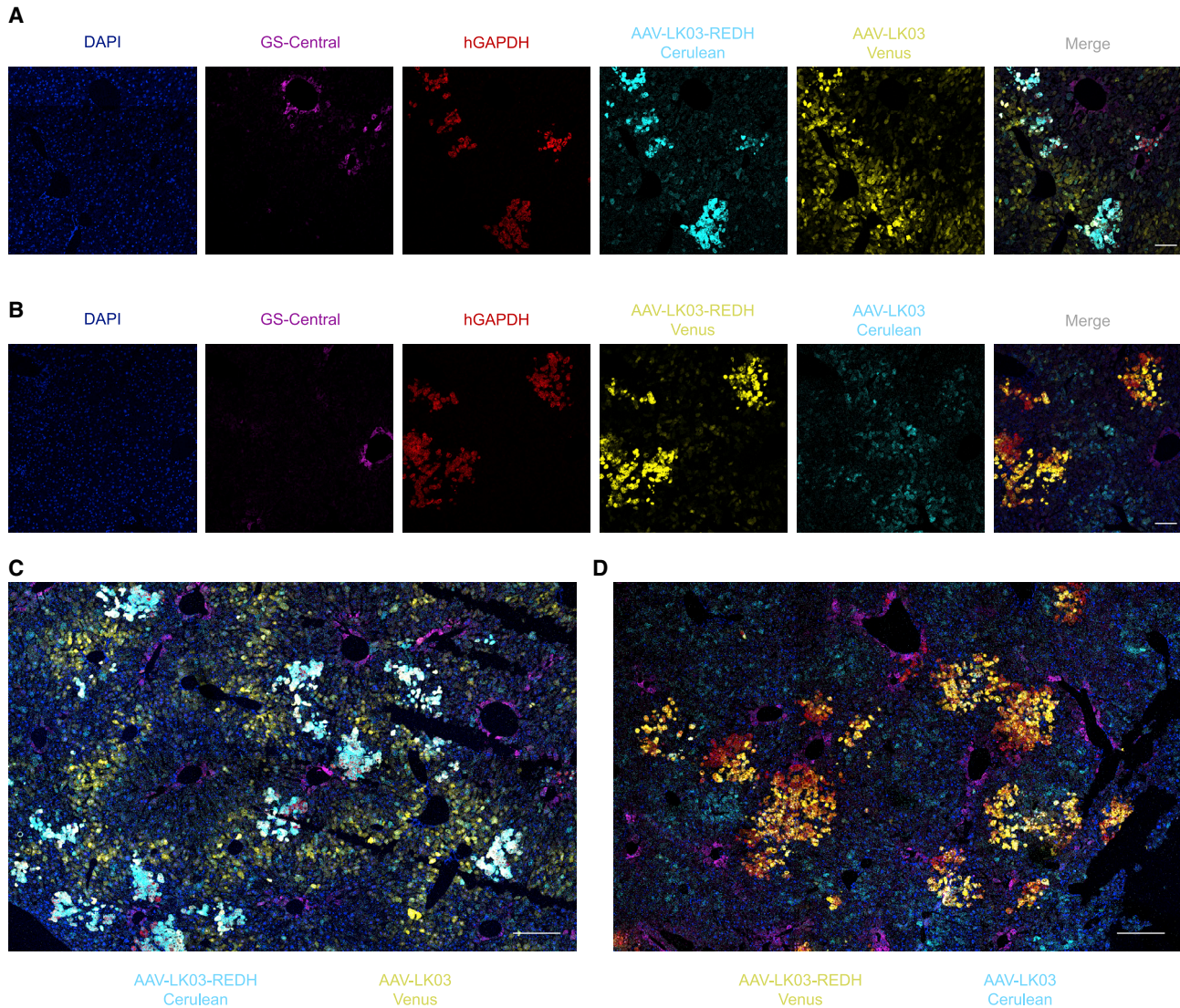
Figure 4. Immunofluorescence analyses of low-engrafted FRG mice transduced with AAV-LK03 and AAV-LK03-REDH vectors encoding for paired Venus and Cerulean fluorophores

(A and C) Representative immunofluorescence analysis of a humanized FRG (hFRG) mouse liver transduced with AAV-LK03-REDH encoding for Cerulean and AAV-LK03 encoding for Venus. (B and D) Representative immunofluorescence analysis of an hFRG mouse liver transduced with AAV-LK03-REDH encoding for Venus and AAV-LK03 encoding for Cerulean. Pericentral hepatocytes are marked with glutamine synthetase (GS, purple). Human clusters are marked with GAPDH (red). Scale bars, 100 μm (A and B) and 200 μm (C and D).

were transduced with AAV compared with the central hepatocytes. This was readily observable in the hFRGs injected with AAV-LK03 encoding for Venus (Figure 7E, right column). As shown in Figures 7D and 7E, the HSPG de-targeted AAV-LK03-REDH transduced a larger proportion of hepatocytes, confirming a generally improved transduction efficiency of AAV-LK03-REDH in this model (Tables S4–S6).

With regard to the transcriptional effects of AAV delivery and cargo expression in primary human hepatocytes 1 week post injection, we compared first the mean expression of genes involved in the p53/Akt

signaling pathway in the primary human liver cells (n = 2) used to repopulate the FRG mice (the "pre-engraftment" sample) and in the control hFRGs that did not receive any AAVs ("engrafted," n = 2, Figure 7F). Interestingly, we found Cdkn1a (p21) to be upregulated in the pre-engraftment samples. This could be linked to the human liver perfusion strategy utilized to isolate single cells before freezing and distribution.

Given the possibility that because of dropout events[42] some nuclei containing AAV transcripts could be scored as untransduced, which could affect the analysis, we decided to compare the human nuclei with
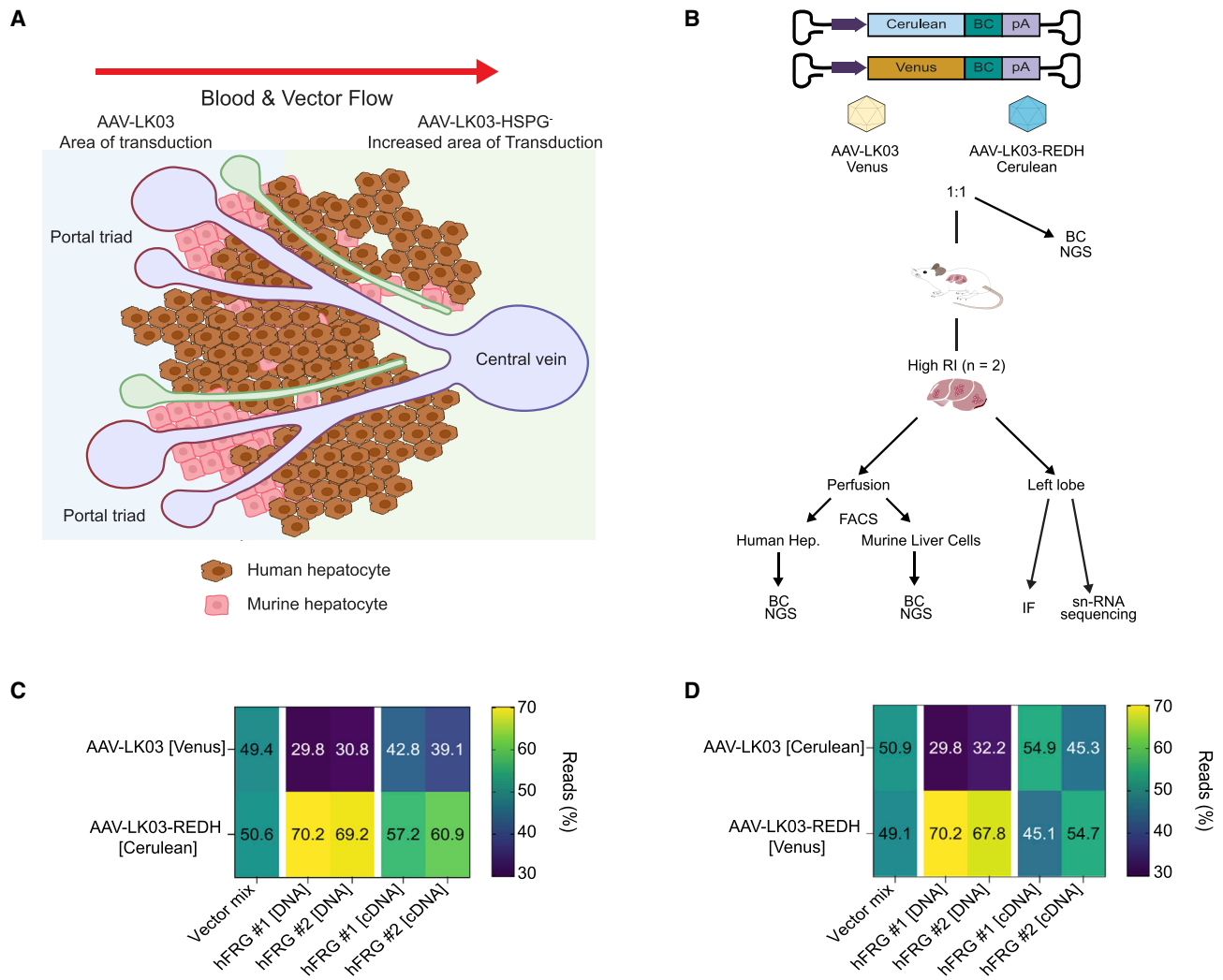
Figure 5. Comparison of AAV-LK03 and AAV-LK03-REDH in highly engrafted humanized FRG mice

(A) Schematic representation of the proposed transduction model for AAV-LK03 and the HSPG de-targeted AAV-LK03 variants in highly engrafted mice. Although the amenable area for transduction for AAV-LK03 is hypothesized to remain like that of Figure 3A, more human hepatocytes are expected to randomly fall under the portal area (blue background) in highly engrafted FRG mice. (B) Schematic representation of the study design comparing AAV-LK03 and AAV-LK03-REDH in highly engrafted mice. (C and D) *In vivo* comparison of AAV-LK03 and AAV-LK03-REDH in highly engrafted animals. Normalized percentage of NGS reads mapped to each capsid in human hepatocytes at the DNA and cDNA are shown (n = 2). In (C), AAV-LK03 was encoded for Venus and AAV-LK03-REDH for Cerulean. The opposite mix was generated for (D).

detectable AAV transcripts ("transduced") with true negative nuclei from the non-injected, engrafted control animal ("engrafted," Figure 7G). As shown in Table S7 and Figure 7G, 1 week after injection we observed significant upregulation of *Mdm2* and *Cdkn1a* and a slight but statistically significant upregulation of *Phlda3* and its effectors *Bax* and *Aen*, although to a lesser extent, in the transduced nuclei. However, we did not observe a significant difference in the expression of p53 (*TP53*) between "transduced" and "engrafted" human hepatocyte nuclei (Figure 7G and Table S7).

Finally, and given the relevance of the vector immune profile for clinical applications, we tested ten human sera for their reactivity to AAV-LK03 and AAV-LK03-REDH with an enzyme-linked immunosorbent assay (ELISA). Five of the ten (50%) were non-reactive to AAV-LK03-REDH, while only three (30%) were non-reactive to AAV-LK03. However, the two sera that were only reactive to AAV-LK03 showed weak reactivity, and thus potentially a larger sample size would be required to categorically state that there is any significant difference between those two variants with regard to immunoreactivity (Figure S9).

DISCUSSION

Recombinant AAV vectors developed from the natural serotypes have provided positive therapeutic outcomes for several genetic
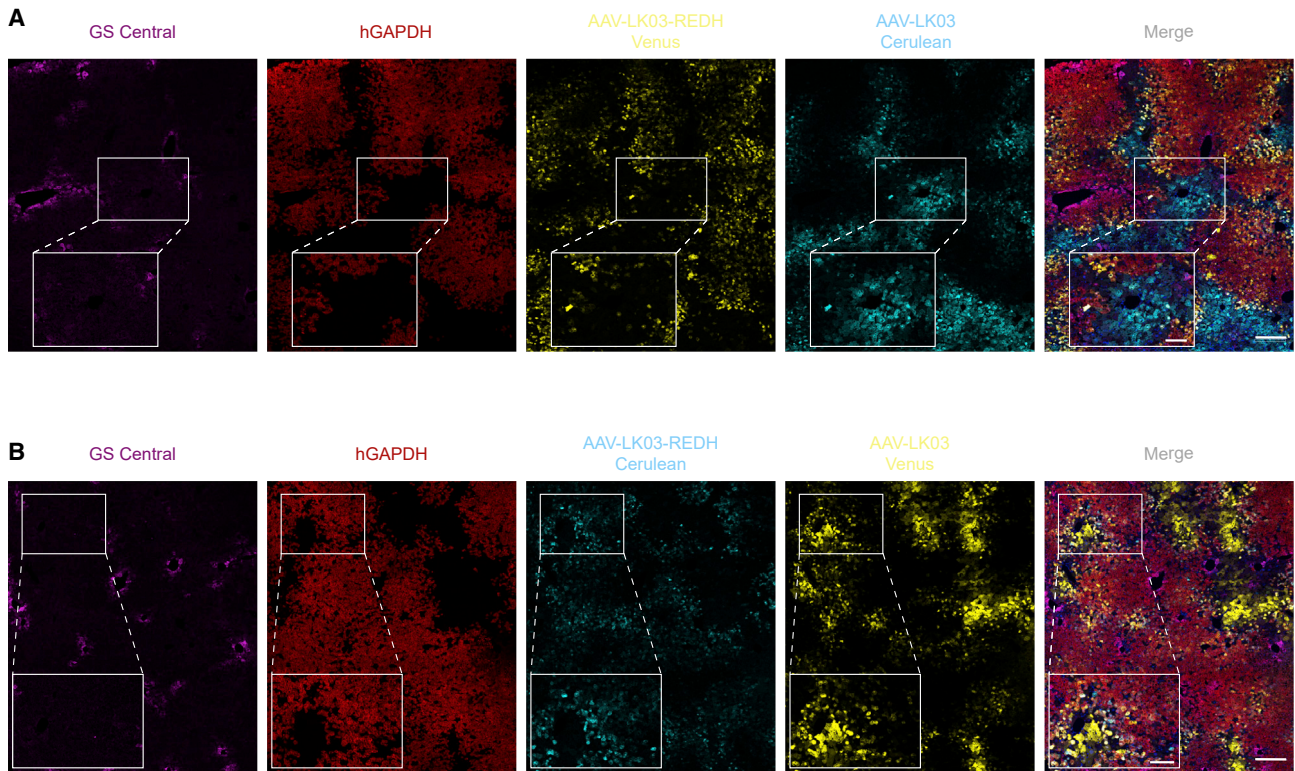
Figure 6. Immunofluorescence analyses of highly engrafted FRG mice transduced with AAV-LK03 and AAV-LK03-REDH vectors encoding for paired Venus and Cerulean fluorophores

(A) Representative immunofluorescence analysis of a humanized FRG (hFRG) mouse liver transduced with AAV-LK03-REDH encoding for Venus and AAV-LK03 encoding for Cerulean. (B) Representative immunofluorescence analysis of an hFRG mouse liver transduced with AAV-LK03-REDH encoding for Cerulean and AAV-LK03 encoding for Venus. Pericentral hepatocytes are marked with glutamine synthetase (GS, purple). Human clusters are marked with GAPDH (red). Scale bars, 500 μm (main figures) and 250 μm (magnified insets).

indications.[43] During the past 25 years, a new generation of engineered AAV vectors has been developed to enhance targeting specificity, safety, and endurance.[43] Until recently, this quest for novel capsids has mainly been directed at particular organs as a whole. However, with the advent of sc-RNA-seq, we can now develop and profile AAV variants across cell types, which is especially important in organs with complex cell-type compositions such as the liver,[44] the retina,[45] or the brain.[46]

Previous studies have also explored single-cell sequencing in AAV development.[44–46] Given the inherent complexity of the xenograft hFRG model, where both human and murine cell types co-exist in the murine liver scaffold, we opted for sn-RNA-seq instead of sc-RNA-seq.[22] By snap-freezing the liver tissue and extracting and sorting the nuclei *a posteriori*, it is possible to minimize the biases introduced by collagenase-based cell dissociation, both at the level of cell-type representation and the level of *de novo* transcriptional stress responses.[28,29] One caveat when using sn-RNA-seq could be related to the relatively lower amount of AAV transgene transcripts present in nuclei than in the cytoplasm. In our case, we detected AAV transgenes in ~9% to ~17% of the human nuclei (Tables S3

and S4). These numbers are likely to be an underestimation because many transcripts are missed in sn-RNA-seq, especially those genes presenting a lower expression magnitude in comparison. We hypothesize that this effect influences the number of AAV transcripts.[42] Strategies to retain the whole or part of the transcript at the nuclei could be explored, such as including long non-coding RNA sequences that promote nuclear enrichment.[47] However, the effect of such sequences on AAV-genome processing and stability would also have to be considered, adding another level of complexity and uncertainty.

We believe the complementary analyses presented here offer a robust approach for assessing AAV transduction in complex organs or models such as the hFRG. De-targeting AAV-LK03 from HSPG yielded a vector that consistently transduced a larger area of the chimeric liver in hFRG, as validated by complementary strategies including NGS (Figure 5), immunofluorescence (Figure 6), and sn-RNA-seq (Figure 7). We have previously reported the same mechanism for AAV2-based vectors in the hFRG model,[16] which is yet another piece of evidence supporting the findings of the current study. It is also important to note the striking difference in relative vector performance between mice presenting low (Figure 4) and
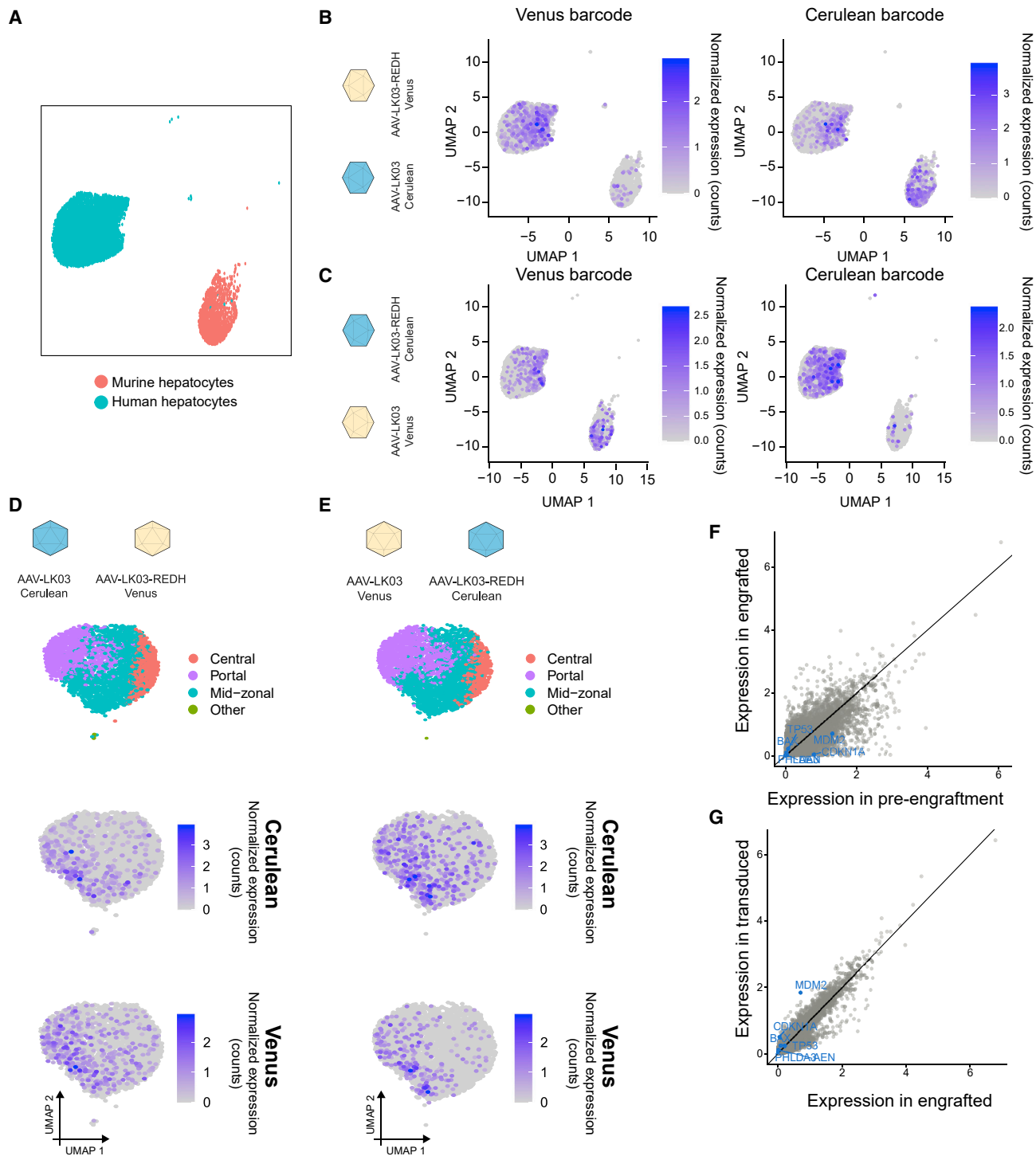
Figure 7. Single-nucleus RNA-sequencing analysis of human and murine nuclei transduced with barcoded AAV-LK03 and AAV-LK03-REDH vectors

(A) UMAP visualization of single human and murine hepatocyte nuclei. (B and C) Expression of Venus and Cerulean in UMAP space in human and murine nuclei analyzed for hFRG injected with indicated complementary fluorophores (n = 2 per condition). (D and E) Log-normalized expression of Venus and Cerulean in human hepatocyte nuclei from hFRG injected with the indicated complementary fluorophores. Identified zonation clusters are indicated in each UMAP plot (top panel). (F) Average log-normalized expression of genes in human nuclei analyzed pre-engraftment (x axis) and in the non-transduced, engrafted control (y axis). Expression levels of *Mdm2* and *Cdkn1a*, and of *Phlda3* and its effectors *Bax*, *Aen*, and *TP53*, in both samples, are highlighted in blue. (G) Similar analysis as shown in (F), comparing expression in engrafted human nuclei (x axis) and in AAV-transduced human nuclei (y axis).

high (Figure 6) RIs. In the former, practically all the human hepatocytes could be transduced with AAV-LK03-REDH. This is likely, at least partially, due to a larger number of vector particles per human hepatocyte (MOT), given that in highly repopulated mice, AAV-LK03-REDH transduction was more apparent at the edges of the human clusters adjacent to the portal area, where the vector first encountered this cell type. How this effect translates across species remains to be studied in larger animal models and eventually in the clinical setting. In addition, different species probably present different extracellular matrix compositions/HSPG profiles, and thus a fine-tuning of the methodology could be required to achieve the maximum functional benefit.

The differential pattern of AAV-mediated transgene expression across the murine hepatic lobule was first described for AAV8 by Cunningham and colleagues in 2008.[48] From the beginning, it was postulated that this could be caused by two non-exclusive processes: preferential vector tropism for specific hepatocytes and promoter specificity. HSPG-binding vectors such as AAV2, AAV3b, and related bioengineered variants such as AAV-KP1 and AAV-LK03 display a marked periportal profile in the hFRG model. Therefore we hypothesize that, in the instance of HSPG-binding capsids, physical restriction of the amenable area for transduction is the primary determinant of this phenomenon.[14,15] In support of our hypothesis, Dane and colleagues also reported a clear periportal bias for AAV2 in the murine liver, where the relative number of vector genomes in the periportal area was five times higher than that in the perivenous area in female mice.[15] In contrast to HSPG-binding vectors, AAV7, AAV8, AAV9, and AAVrh10 exhibit a predominantly perivenous pattern in the murine liver,[15] which also correlates with more vector genomes in the pericentral region of the lobule.[48] Bell and colleagues also reported this pericentral dominance in transgene expression in mice with AAV8 encoding transgenes under three different promoters, suggesting that transduction zonation is not caused by promoter specificity.[49] However, we have recently described wide lobular transduction with the murine tropic AAV-LK03-265*ins*T-R595G[14] encoding for the ssAAV-LSP1-GFP-BC-WPRE-BGHpA. However, the same vector packaged with a cassette containing the human cytomegalovirus promoter resulted in a marked pericentral expression profile.[14] Given that the capsid was kept constant, our data suggest that, in some instances, promoters can also have a determining role in differential transgene expression across the hepatic lobule, in agreement with the initial postulate by Cunningham et al.[48]

Interestingly, a predominantly pericentral expression was also found in dogs injected with AAV8,[49] although the same authors found the pattern reversed in cynomolgus and rhesus macaques, where the transgene expression was most intense around the portal vein.[49] Although the mechanism responsible for these differences is currently unknown, we think it could be influenced by the different affinities of AAV8 to murine and non-human primate AAVRs.[31] It is plausible that being of non-human primate origin, AAV8 presents a higher affinity for the non-human primate AAVR, which could, in turn, shift its lobular transduction profile to the periportal zone first encountered by AAVs entering hepatic lobule with the blood. Differences in matrix proteoglycan compositions between mice and non-human primates, or even of AAVR distribution across the hepatic lobule, could also account for these transduction disparities, as has recently been hypothesized.[50]

An interesting phenomenon in our study related to transgene expression was that the double mutant AAV-LK03-REDH (R594E + D598H) presented reduced functional transduction (RNA output per DNA input) compared with its parental AAV-LK03. This was especially noticeable in murine hepatocytes, where although we could map a larger amount of DNA reads to AAV-LK03-REDH, this mutant was not functional in murine cells (Figures 3D and 3E). To a lesser extent, we also detected a loss in functional performance in human hepatocytes. We hypothesize that this observation could be explained by at least three possible and not mutually exclusive mechanisms. First, we cannot exclude the possibility of the lower RNA output being related to an unidentified impairment of a post-entry, but pre-transcription, step. Another intriguing possibility could be the presence of a minimum required threshold of transgenes per cell to reach functional transduction, given that the de-targeted variant physically transduces a larger number of cells but at a lower average vg count per cell, whereas canonical AAV-LK03 does the opposite. Finally, given that this comparison is performed at a particular time point (1 week post injection), it is also possible that the observed differences reflect differential post-entry kinetics of the variants. Further studies will be required to better understand the underlying mechanism.

In summary, we have provided further evidence that fine-tuning the HSPG attachment profile of AAV vectors can be a powerful tool for engineering their liver lobular transduction profiles. It is crucial to note that in some instances, such as when treating metabolic diseases that affect hepatocytes in specific hepatic zones,[51] it might be beneficial to deliberately select a vector presenting a marked periportal or pericentral profile. In other instances, for example when expressing therapeutic proteins released by the cells, such as coagulation factors in the case of hemophilia A or B, a wider vector distribution might allow reduction of liver damage associated with a toxic level of high vector copies per cell. Although we performed this proof of concept in a pre-clinical humanized mouse model, we hypothesize that the same mechanism could be exploited to generate AAV vectors with wider lobular transduction in larger animals and, eventually, humans. Furthermore, similar mechanisms could be explored to improve gene therapy vectors targeting other organs and tissues, where interactions with extracellular matrix and HSPG could directly affect vector distributions and, thus, clinical utility.

MATERIALS AND METHODS
Mouse studies and isolation of human hepatocytes by collagenase perfusion
All animal experimental procedures and care were approved by the joint Children's Medical Research Institute (CMRI) and The Children's Hospital at Westmead Animal Care and Ethics Committee.

Fah$^{-/-}$Rag2$^{-/-}$Il2rg$^{-/-}$ (FRG) mice were bred, housed, engrafted, and monitored as recently described.[37] Levels of human cell engraftment were estimated by measuring the presence of human albumin in peripheral blood, using the human albumin ELISA quantitation kit (Bethyl Laboratories; #E80-129). To evaluate the AAV transduction potential, mice were placed on 10% NTBC and were maintained in this condition until harvest. All hFRG mice reported in this study were engrafted with hepatocytes from the same human donor (Caucasian, 15-month-old donor; Lonza; #HUM181791).

Mice were randomly assigned to experiments and transduced via intravenous injection (lateral tail vein) with the indicated vector doses. Mice were euthanized by CO$_2$ inhalation either 1 week after transduction for barcoded NGS analyses, immunohistochemistry studies, and sn-RNA-seq. To obtain murine and human single-cell suspensions from xenografted murine livers, we followed the same collagenase perfusion procedure as recently described.[37] In brief, cells were labeled with phycoerythrin (PE)-conjugated anti-human-HLA-ABC (clone W6/32, Invitrogen #12-9983-42; 1:20), biotin-conjugated anti-mouse-H-2Kb (clone AF6-88.5, BD Pharmigen #553568; 1:100), and allophycocyanin (APC)-conjugated streptavidin (eBioscience #17-4317-82; 1:500). Flow cytometry was performed in the Flow Cytometry Facility, Westmead Institute for Medical Research (Westmead, NSW, Australia). The data were analyzed using FlowJo 7.6.1 (FlowJo).

To obtain samples from the same animals for immunofluorescence and sn-RNA-seq analyses, we tightened the left lobe of the studied FRG livers prior to collagenase perfusion. For sn-RNA-seq experiments we flash-froze ~25-mg liver chunks from the left lobe, and for immunofluorescence analyses we proceeded as indicated in the corresponding section.

Lentiviral vector packaging

LeGO-Cer2, LeGO-C2, and LeGO-V2[34] were modified to include the puromycin resistance gene and were produced by transient transfection of HEK293T packaging cells, using the third-generation lentiviral packaging plasmids pRRE and pRSV-Rev.2, and the Env plasmid VSV-G. Supernatants containing lentiviral particles were concentrated using two rounds of ultracentrifugation, and vector particles were titrated by transduction of HEK293T cells in the presence of 8 μg/mL Polybrene. Gene transfer rates by each LeGO lentiviral vector were analyzed at 72 h post transduction by flow cytometry.

Isolation of FRG passage 1 human hepatocytes

We followed the same collagenase perfusion procedure as recently described[37] to obtain murine and human single hepatocyte suspensions from xenografted FRG livers. Human hepatocytes were separated from mouse with EasySep Mouse Streptavidin RapidSpheres Isolation Kit (STEMCELL Technologies; #19860). To check the purity of human hepatocyte fraction, we labeled the cells with PE-conjugated anti-human-HLA-ABC, biotin-conjugated anti-mouse-H-2Kb, and APC-conjugated streptavidin.

Culturing conditions and lentiviral transduction of passage 1 human hepatocytes

In vitro culture of P1 human hepatocytes was performed as described recently.[52] In brief, cryopreserved P1 human hepatocytes were thawed, counted in trypan blue, and plated on a collagen-coated plate (Gibco; #A1142802) in W10 plating medium (William's E medium [WEM], Gibco; #12551032) supplemented with 10% fetal bovine serum, 1% penicillin/streptomycin (Sigma; #P4333), 1% 200 mM L-glutamine (Gibco; #25030149), 0.1% 50 mg/mL gentamicin reagent solution (Gibco; #15710064), and 0.1% ITS (Sigma; I3146). After overnight incubation in humidified 37°C incubator, hepatocytes were washed once with WEM and maintained in hepatocyte-defined medium (Lonza; #185319), supplemented with 1% penicillin/streptomycin, 1% 200 mM L-glutamine, 0.1% 50 mg/mL gentamicin, and 2% dimethyl sulfoxide (Sigma; #D2650); maintenance medium was changed every second day. Twenty-four hours after seeding, confluent P1 hepatocytes were transduced with LeGO-Cer2, LeGO-C2, and LeGO-V2 lentiviral vectors at multiplicity of infection of 0.7 in the presence of 8 μg/mL Polybrene by spinoculation for 30 min at 1,000 × *g* at 25°C. Five days after lentiviral transduction, Cerulean, mCherry, and Venus fluorescent protein-expressed hepatocytes were selected by addition of puromycin (Gibco; #A1113803) in maintenance medium to the final concentration of 2 μg/mL. Seventy-two hours after puromycin selection, hepatocytes were washed with WEM, incubated for 30 min with Hanks' balanced salt solution with 10-min interval washes to loosen tight junctions, and detached from collagen-coated plates by incubation with TrypLE Select (10×; Gibco; #A12177-01) for 5 min; after being gently resuspended in W10 medium, cells were spun at 50 × *g*, resuspended, counted in trypan blue, and re-engrafted into an FRG recipient mouse.

ELISA measurement of anti-AAV IgG-specific antibody titer in human serum

Ten human sera were assayed for reactivity to AAV-LK03 and AAV-LK03-REDH by ELISA. Ninety-six-well polystyrene ELISA plates (Nunc; #442404) were coated overnight at 4°C with 50 μL per well of AAV vector stocks (2.5 × 10^{10} vg/mL) diluted in coating buffer (carbonate-bicarbonate buffer, Sigma-Aldrich). Plates were washed three times with wash buffer (PBS) + 0.05% Tween 20 (Sigma-Aldrich) and then received 100 μL per well of blocking buffer (PBS + 5% skim milk + 0.05% Tween 20). Plates were then washed three times after incubation at room temperature for 2 h in wash buffer and received 50 μL per well of sera (diluted in blocking buffer at 1:50, with duplicate wells for each dilution). Plates were incubated for 2 h at room temperature and washed three times with wash buffer before receiving 50 μL per well of horseradish peroxidase-conjugated anti-human Fc-specific IgG (Chemicon AP309P, diluted 1:10,000 in blocking buffer). Plates were incubated for 1 h at room temperature and washed four times using wash buffer before receiving 75 μL per well of 3,3′,5,5′-tetramethylbenzidine (Sigma-Aldrich). Plates were incubated in the dark for 30 min at room temperature, and the reactions were then stopped using 75 μL per well of 1 M sulfuric acid. The absorbance of each well was measured at 450-nm wavelength using a VersaMax microplate reader (Molecular Devices).

Duplicate wells containing no AAV served as background controls. The mean value for each sample dilution was calculated for wells with coated vector (foreground) and without coated vector (background), and the sample was considered reactive if this ratio was >2.0.

Immunofluorescence analysis of humanized FRG mouse livers
Immunofluorescence was performed as described in detail recently without modifications.[37] In brief, mouse livers were fixed with paraformaldehyde, cryoprotected in sucrose, and frozen in OCT (Tissue-Tek). Frozen liver sections (5 μm) were permeabilized in ice-cold methanol followed by room-temperature 0.1% Triton X-100, then reacted with anti-human GAPDH antibody (Abcam; #ab215227) and 4′,6-diamidino-2-phenylindole (Invitrogen; #D1306) at 0.08 ng/mL. When indicated in the figure legends, anti-GS (Origene; #TA500700) was used. For Figure 2A, anti-HAL (Sigma Prestige Antibodies; #HPA038547), anti-ASL (Invitrogen; #PA5-22300), anti-ASS (Invitrogen; #PA5-82740), and anti-CPS1 (Abcam; #ab129076) antibodies were used as indicated. For Figures 2B and 2D, anti-cytokeratin 7 (Abcam; #ab68459) was used. After immunolabeling, the images were captured and analyzed on an LSM800-Airyscan microscope using ZEN Black software.

Nuclei isolation
Hepatic nuclei were isolated directly from the commercial Lonza vial or from flash-frozen liver chunks as described in detail recently[22] with no further modifications.

Single-nucleus RNA library preparation and sequencing
For the construction of sn-RNA-seq libraries, 10x Genomics Chromium Single Cell 3′v3 Reagent Kits were used according to the manufacturer's instructions. Libraries were prepared as described recently,[22] with no further modifications.

sn-RNA-seq data processing and analysis
Data were acquired on a NovaSeq6000 instrument in BCL format. These files were de-multiplexed and converted into FASTQ format using the bcl2fastq tool in Illumina BaseSpace Sequence Hub. CellRanger 6.0.0 with "–include-introns" option was used to process the FASTQ files, using a custom reference built from the human (refdata-gex-GRCh38-2020-A) and mouse (refdata-gex-mm10-2020-A) 10x Genomics references, as well as the AAV transgene barcodes. The resulting gene-barcode matrices were analyzed using Seurat (version 4.0.5).[53] When analyzing only human gene expression, mouse genes were excluded before creating a Seurat object, and nuclei were included if they had at least 2,000 but no more than 7,000 genes expressed, as well as fewer than 0.3% mitochondrial gene expression.

For identification of liver cell types, human gene expression data were integrated with a pre-processed dataset from Aizarani et al.,[13] downloaded from the Gene Expression Omnibus (GEO: GSE124395) in RData format. The gene-barcode matrix for normal human liver cells was downloaded and processed using the standard Seurat pipeline (normalization, identification of variable features, scaling, principal component analysis [PCA], UMAP, identification of neighbors and clusters). Inspection of the Seurat-defined clusters revealed that cell types annotated in the GEO data did not always cluster together, so cell types were assigned to clusters by inspecting the expression of marker genes for each cell type (identified from both the original publication and PanglaoDB).[41] These cell types were then identified in the human gene expression data by integrating[23] our data with the Aizarani dataset[13] using the FindTransferAnchors and MapQuery functions.

For identification of zonation in human hepatocytes, the datasets containing human genes were integrated together using the SelectIntegrationFeatures, FindIntegrationAnchors, and IntegrateData functions, followed by the standard Seurat workflow (scaling, PCA, UMAP, neighbor identification, and clustering). Marker genes differentially expressed between clusters were identified using the FindAllMarkers function, using the Wilcoxon rank-sum test, for genes that were expressed in at least 25% of the cells in each cluster and a log fold change of at least 0.25 compared with all remaining cells. The Wilcoxon rank-sum test was also used to compare the differential expression of genes of interest between clusters or treatments. In addition, the expression of well-known zonation genes were inspected in violin and UMAP plots.

For comparison of mouse and human hepatocyte transduction, mouse genes were retained, and nuclei were included if they had at least 2,000 but no more than 6,000 genes expressed, and fewer than 0.5% mitochondrial gene expression. Datasets were integrated together in the same way as described above, before processing using the standard Seurat workflow. The Wilcoxon rank-sum test was used to examine the differential expression of genes between clusters and treatment groups.

DNA and RNA isolation, and cDNA synthesis
Isolation of DNA and RNA, and cDNA synthesis were performed as described in detail previously[18] with no further modifications. In brief, DNA was extracted using a standard phenol/chloroform protocol and RNA with the Direct-Zol kit (Zymogen; #R2062). cDNA synthesis was carried out with SuperScript IV first-strand synthesis (Invitrogen), following the manufacturer's instructions.

Heparin-binding assay
The heparin affinity of the described AAV-LK03 variants was determined using a 1-mL HiTrap Heparin HP column (Cytiva; #17040601) on an AKTA pure 25 M2 fast protein liquid chromatography system, as described in detail in a previous publication.[37]

AAV packaging
AAV constructs were packaged into AAV capsids using HEK293 cells and a helper-virus-free system, as described previously.[54] Genomes were packaged in capsid variants using packaging plasmid constructs harboring rep genes from AAV2 and a specific capsid. Packaging of multiple barcoded ss-LSP1-eGFP-BC-WPRE-BGHpA was achieved, as described recently.[16] All vectors/libraries were purified using iodixanol gradient ultracentrifugation, as previously described.[55] AAV

preparations were titered using droplet digital PCR (ddPCR; see AAV titration for details).

AAV transgene constructs

All vectors used in the study contain AAV2 ITR sequences. The AAV construct pLSP1-eGFP-WPRE-BGHpA, which encodes eGFP under the transcriptional control of a heterologous promoter containing one copy of the SERPINA1 (hAAT) promoter and two copies of the apolipoprotein E enhancer element, has been previously reported.[56] The barcoded versions of this construct include a 6-mer barcode between eGFP and WPRE.[18] The Venus and Cerulean transgenes were cloned into a self-complementary, CAG-driven plasmid (Addgene; #83279[40]) by substituting eGFP for either transgene encoding for each fluorophore. The plasmids encoding for Venus and Cerulean were kindly provided by Dr. Grant Logan. The barcoded constructs of these transgenes contain a 50-mer-long barcode between the phlorophore and the Simian virus 40 (SV40) polyadenylation tail as indicated below. Venus: 5′-GCG AGC CGC CGA TCT ACT GAG ACA GCG AGC GTT CCA TCG TTC TTT CTT CG-3′; Cerulean: 5′- TCA GAG TCC CTC GCA TCG CCT GCG CTC CCT CCG CAG TTT TCC TTG CGG GG-3′.

AAV titration

AAV titration was performed via ddPCR (Bio-Rad) using EvaGreen Supermix (Bio-Rad; #1864034) and following the manufacturer's instructions. To detect AAV genomes on vectors, GFP primers were used (GFP-F: 5′-TCA AGA TCC GCC ACA ACA TC; GFP-R: 5′-TTC TCG TTG GGG TCT TTG CT).

Barcode amplification, NGS, and distribution analysis

For Figure 3B, the 150-bp region surrounding the 6-mer barcode was amplified with Q5 High-Fidelity DNA Polymerase (NEB; #M0491L) using BC_F (5′-GCT GGA GTT CGT GAC CGC CG) and BC_R primer (5′-CAA CAT AGT TAA GAA TAC CAG TCA ATC TTT CAC AAA TTT TGT AAT CCA GAG G). For Venus and Cerulean barcode sequencing, BC-Ven_Cer_F (5′-TTC GTG ACC GCC GCC GGG ATC) and BC-Ven_Cer_R (5′-CAC AAA TAA AGC ATC GAG ATC GCA GGT GAG GCC) were used instead.

NGS library preparations and sequencing using 2×150 paired-end configurations were performed by Genewiz (Suzhou, China) using an Illumina MiSeq instrument. A workflow was written in Snakemake (5.6)42 to process reads and count barcodes. Paired reads were merged using BBMerge and then filtered for reads of the expected length in a second pass through BBDuk, both from BBTools 38.68 (https://sourceforge.net/projects/bbmap/). The merged, filtered fastq files were passed to a Python (3.7) script that identified barcodes corresponding to AAV variants. NGS reads from the DNA and cDNA populations were normalized to the reads from the pre-injection vector mix.

DATA AVAILABILITY

Raw data (FASTQ files) and processed gene-barcode matrices for the sn-RNA-seq experiments are available in the GEO (GEO:

GSE207809). Code is available on GitHub (https://doi.org/10.5281/zenodo.6615734).

SUPPLEMENTAL INFORMATION

Supplemental information can be found online at https://doi.org/10.1016/j.omtm.2022.12.014.

AUTHOR CONTRIBUTIONS

Conceptualization, M.C.-C. and L.L.; methodology, M.C.-C., R.G.N., S.H.Y.L., R.C., and E.Z.; software, S.S., R.C., M.J., E.D., A.R.R.F., and J.E.E.T.-P.; investigation, M.C.-C., R.G.N., S.H.Y.L., R.C., M.K., and G.B.; writing – original draft, M.C.-C.; writing – review and editing, M.C.-C., S.S., and L.L.; funding acquisition, I.E.A., J.E.E.T.-P., and L.L.; visualization, M.C.-C. and R.R.-P.; supervision, M.C.-C. and L.L.

DECLARATION OF INTERESTS

L.L. is a cofounder of LogicBio Therapeutics, and L.L. and I.E.A. are co-founders of Exigen Biotherapeutics, companies that utilize similar technologies broadly discussed in this paper.

REFERENCES

1. Gao, G., Vandenberghe, L.H., Alvira, M.R., Lu, Y., Calcedo, R., Zhou, X., and Wilson, J.M. (2004). Clades of Adeno-associated viruses are widely disseminated in human tissues. J. Virol. 78, 6381–6388. https://doi.org/10.1128/JVI.78.12.6381-6388.2004.

2. Sonntag, F., Köther, K., Schmidt, K., Weghofer, M., Raupp, C., Nieto, K., Kuck, A., Gerlach, B., Böttcher, B., Müller, O.J., et al. (2011). The assembly-activating protein promotes capsid assembly of different adeno-associated virus serotypes. J. Virol. 85, 12686–12697. https://doi.org/10.1128/JVI.05359-11.

3. Ogden, P.J., Kelsic, E.D., Sinai, S., and Church, G.M. (2019). Comprehensive AAV capsid fitness landscape reveals a viral gene and enables machine-guided design. Science 366, 1139–1143. https://doi.org/10.1126/science.aaw2900.

4. Wörner, T.P., Bennett, A., Habka, S., Snijder, J., Friese, O., Powers, T., Agbandje-McKenna, M., and Heck, A.J.R. (2021). Adeno-associated virus capsid assembly is divergent and stochastic. Nat. Commun. 12, 1642. https://doi.org/10.1038/s41467-021-21935-5.

5. Li, C., and Samulski, R.J. (2020). Engineering adeno-associated virus vectors for gene therapy. Nat. Rev. Genet. *21*, 255–272. https://doi.org/10.1038/s41576-019-0205-4.

6. Stemmer, W.P. (1994). DNA shuffling by random fragmentation and reassembly: in vitro recombination for molecular evolution. Proc. Natl. Acad. Sci. USA *91*, 10747–10751. https://doi.org/10.1073/pnas.91.22.10747.

7. Grimm, D., Lee, J.S., Wang, L., Desai, T., Akache, B., Storm, T.A., and Kay, M.A. (2008). In vitro and in vivo gene therapy vector evolution via multispecies interbreeding and retargeting of adeno-associated viruses. J. Virol. *82*, 5887–5911. https://doi.org/10.1128/JVI.00254-08.

8. Lisowski, L., Dane, A.P., Chu, K., Zhang, Y., Cunningham, S.C., Wilson, E.M., Nygaard, S., Grompe, M., Alexander, I.E., and Kay, M.A. (2014). Selection and evaluation of clinically relevant AAV variants in a xenograft liver model. Nature *506*, 382–386. https://doi.org/10.1038/nature12875.

9. Azuma, H., Paulk, N., Ranade, A., Dorrell, C., Al-Dhalimy, M., Ellis, E., Strom, S., Kay, M.A., Finegold, M., and Grompe, M. (2007). Robust expansion of human hepatocytes in Fah-/-/Rag2-/-/Il2rg-/- mice. Nat. Biotechnol. *25*, 903–910. https://doi.org/10.1038/nbt1326.

10. George, L.A., Monahan, P.E., Eyster, M.E., Sullivan, S.K., Ragni, M.V., Croteau, S.E., Rasko, J.E.J., Recht, M., Samelson-Jones, B.J., MacDougall, A., et al. (2021). Multiyear factor VIII expression after AAV gene transfer for hemophilia A. N. Engl. J. Med. *385*, 1961–1973. https://doi.org/10.1056/NEJMoa2104205.

11. Jungermann, K., and Kietzmann, T. (1996). Zonation of parenchymal and nonparenchymal metabolism in liver. Annu. Rev. Nutr. *16*, 179–203. https://doi.org/10.1146/annurev.nu.16.070196.001143.

12. Gebhardt, R. (1992). Metabolic zonation of the liver: regulation and implications for liver function. Pharmacol. Ther. *53*, 275–354. https://doi.org/10.1016/0163-7258(92)90055-5.

13. Aizarani, N., Saviano, A., Sagar, Mailly, L., Durand, S., Herman, J.S., Pessaux, P., Baumert, T.F., and Grün, D. (2019). A human liver cell atlas reveals heterogeneity and epithelial progenitors. Nature *572*, 199–204. https://doi.org/10.1038/s41586-019-1373-2.

14. Cabanes-Creus, M., Navarro, R.G., Liao, S.H.Y., Baltazar, G., Drouyer, M., Zhu, E., Scott, S., Luong, C., Wilson, L.O.W., Alexander, I.E., and Lisowski, L. (2021). Single amino acid insertion allows functional transduction of murine hepatocytes with human liver tropic AAV capsids. Mol. Ther. Methods Clin. Dev. *21*, 607–620. https://doi.org/10.1016/j.omtm.2021.04.010.

15. Dane, A.P., Wowro, S.J., Cunningham, S.C., and Alexander, I.E. (2013). Comparison of gene transfer to the murine liver following intraperitoneal and intraportal delivery of hepatotropic AAV pseudo-serotypes. Gene Ther. *20*, 460–464. https://doi.org/10.1038/gt.2012.67.

16. Cabanes-Creus, M., Westhaus, A., Navarro, R.G., Baltazar, G., Zhu, E., Amaya, A.K., Liao, S.H.Y., Scott, S., Sallard, E., Dilworth, K.L., et al. (2020). Attenuation of heparan sulfate proteoglycan binding enhances in vivo transduction of human primary hepatocytes with AAV2. Mol. Ther. Methods Clin. Dev. *17*, 1139–1154. https://doi.org/10.1016/j.omtm.2020.05.004.

17. Rutledge, E.A., Halbert, C.L., and Russell, D.W. (1998). Infectious clones and vectors derived from adeno-associated virus (AAV) serotypes other than AAV type 2. J. Virol. *72*, 309–319.

18. Cabanes-Creus, M., Hallwirth, C.V., Westhaus, A., Ng, B.H., Liao, S.H.Y., Zhu, E., Navarro, R.G., Baltazar, G., Drouyer, M., Scott, S., et al. (2020). Restoring the natural tropism of AAV2 vectors for human liver. Sci. Transl. Med. *12*, eaba3312. https://doi.org/10.1126/scitranslmed.aba3312.

19. Sugahara, G., Ishida, Y., Sun, J., Tateno, C., and Saito, T. (2020). Art of making artificial liver: depicting human liver biology and diseases in mice. Semin. Liver Dis. *40*, 189–212. https://doi.org/10.1055/s-0040-1701444.

20. Chow, E.C.Y., Wang, J.Z.Y., Quach, H.P., Tang, H., Evans, D.C., Li, A.P., Silva, J., and Pang, K.S. (2016). Functional integrity of the chimeric (humanized) mouse liver: enzyme zonation, physiologic spaces, and hepatic enzymes and transporters. Drug Metab. Dispos. *44*, 1524–1535. https://doi.org/10.1124/dmd.116.070060.

21. Kakuni, M., Yamasaki, C., Tachibana, A., Yoshizane, Y., Ishida, Y., and Tateno, C. (2013). Chimeric mice with humanized livers: a unique tool for in vivo and in vitro enzyme induction studies. Int. J. Mol. Sci. *15*, 58–74. https://doi.org/10.3390/ijms15010058.

22. Carlessi, R., Denisenko, E., Boslem, E., Koehn-Gaone, J., Main, N., Abu Bakar, N.D.B., Shirolkar, G.D., Jones, M., Poppe, D., Dwyer, B.J., et al. (2022). Single nucleus RNA sequencing of pre-malignant liver reveals disease-associated hepatocyte state with HCC prognostic potential. Preprint at bioRxiv. https://doi.org/10.1101/2022.03.25.485695.

23. Stuart, T., Butler, A., Hoffman, P., Hafemeister, C., Papalexi, E., Mauck, W.M., 3rd, Hao, Y., Stoeckius, M., Smibert, P., and Satija, R. (2019). Comprehensive integration of single-cell data. Cell *177*, 1888–1902.e21. https://doi.org/10.1016/j.cell.2019.05.031.

24. Halpern, K.B., Shenhav, R., Matcovitch-Natan, O., Toth, B., Lemze, D., Golan, M., Massasa, E.E., Baydatch, S., Landen, S., Moor, A.E., et al. (2017). Single-cell spatial reconstruction reveals global division of labour in the mammalian liver. Nature *542*, 352–356. https://doi.org/10.1038/nature21065.

25. Kietzmann, T. (2017). Metabolic zonation of the liver: the oxygen gradient revisited. Redox Biol. *11*, 622–630. https://doi.org/10.1016/j.redox.2017.01.012.

26. MacParland, S.A., Liu, J.C., Ma, X.Z., Innes, B.T., Bartczak, A.M., Gage, B.K., Manuel, J., Khuu, N., Echeverri, J., Linares, I., et al. (2018). Single cell RNA sequencing of human liver reveals distinct intrahepatic macrophage populations. Nat. Commun. *9*, 4383. https://doi.org/10.1038/s41467-018-06318-7.

27. Braeuning, A., Ittrich, C., Köhle, C., Hailfinger, S., Bonin, M., Buchmann, A., and Schwarz, M. (2006). Differential gene expression in periportal and perivenous mouse hepatocytes. FEBS J. *273*, 5051–5061. https://doi.org/10.1111/j.1742-4658.2006.05503.x.

28. Denisenko, E., Guo, B.B., Jones, M., Hou, R., de Kock, L., Lassmann, T., Poppe, D., Clément, O., Simmons, R.K., Lister, R., and Forrest, A.R.R. (2020). Systematic assessment of tissue dissociation and storage biases in single-cell and single-nucleus RNA-seq workflows. Genome Biol. *21*, 130. https://doi.org/10.1186/s13059-020-02048-6.

29. Wu, H., Kirita, Y., Donnelly, E.L., and Humphreys, B.D. (2019). Advantages of single-nucleus over single-cell RNA sequencing of adult kidney: rare cell types and novel cell states revealed in fibrosis. J. Am. Soc. Nephrol. *30*, 23–32. https://doi.org/10.1681/ASN.2018090912.

30. Wei, Y., Wang, Y.G., Jia, Y., Li, L., Yoon, J., Zhang, S., Wang, Z., Zhang, Y., Zhu, M., Sharma, T., et al. (2021). Liver homeostasis is maintained by midlobular zone 2 hepatocytes. Science *371*, eabb1625. https://doi.org/10.1126/science.abb1625.

31. Pillay, S., Meyer, N.L., Puschnik, A.S., Davulcu, O., Diep, J., Ishikawa, Y., Jae, L.T., Wosen, J.E., Nagamine, C.M., Chapman, M.S., and Carette, J.E. (2016). An essential receptor for adeno-associated virus infection. Nature *530*, 108–112. https://doi.org/10.1038/nature16465.

32. Paku, S., Dezso, K., Kopper, L., and Nagy, P. (2005). Immunohistochemical analysis of cytokeratin 7 expression in resting and proliferating biliary structures of rat liver. Hepatology *42*, 863–870. https://doi.org/10.1002/hep.20858.

33. Sohlenius-Sternbeck, A.K. (2006). Determination of the hepatocellularity number for human, dog, rabbit, rat and mouse livers from protein concentration measurements. Toxicol. Vitro *20*, 1582–1586. https://doi.org/10.1016/j.tiv.2006.06.003.

34. Weber, K., Bartsch, U., Stocking, C., and Fehse, B. (2008). A multicolor panel of novel lentiviral "gene ontology" (LeGO) vectors for functional gene analysis. Mol. Ther. *16*, 698–706. https://doi.org/10.1038/mt.2008.6.

35. Lerch, T.F., and Chapman, M.S. (2012). Identification of the heparin binding site on adeno-associated virus serotype 3B (AAV-3B). Virology *423*, 6–13. https://doi.org/10.1016/j.virol.2011.10.007.

36. Muramatsu, S., Mizukami, H., Young, N.S., and Brown, K.E. (1996). Nucleotide sequencing and generation of an infectious clone of adeno-associated virus 3. Virology *221*, 208–217. https://doi.org/10.1006/viro.1996.0367.

37. Cabanes-Creus, M., Navarro, R.G., Zhu, E., Baltazar, G., Liao, S.H.Y., Drouyer, M., Amaya, A.K., Scott, S., Nguyen, L.H., Westhaus, A., et al. (2022). Novel human liver-tropic AAV variants define transferable domains that markedly enhance the human tropism of AAV7 and AAV8. Mol. Ther. Methods Clin. Dev. *24*, 88–101. https://doi.org/10.1016/j.omtm.2021.11.011.

38. Nagai, T., Ibata, K., Park, E.S., Kubota, M., Mikoshiba, K., and Miyawaki, A. (2002). A variant of yellow fluorescent protein with fast and efficient maturation for cell-biological applications. Nat. Biotechnol. *20*, 87–90. https://doi.org/10.1038/nbt0102-87.

39. Rizzo, M.A., Springer, G.H., Granada, B., and Piston, D.W. (2004). An improved cyan fluorescent protein variant useful for FRET. Nat. Biotechnol. *22*, 445–449. https://doi.org/10.1038/nbt945.

40. Pekrun, K., De Alencastro, G., Luo, Q.J., Liu, J., Kim, Y., Nygaard, S., Galivo, F., Zhang, F., Song, R., Tiffany, M.R., et al. (2019). Using a barcoded AAV capsid library to select for clinically relevant gene therapy vectors. JCI Insight *4*, e131610. https://doi.org/10.1172/jci.insight.131610.

41. Franzen, O., Gan, L.M., and Bjorkegren, J.L.M. (2019). PanglaoDB: A Web Server for Exploration of Mouse and Human Single-Cell RNA Sequencing Data. Database *2019*, baz046. https://doi.org/10.1093/database/baz046.

42. Kharchenko, P.V., Silberstein, L., and Scadden, D.T. (2014). Bayesian approach to single-cell differential expression analysis. Nat. Methods *11*, 740–742. https://doi.org/10.1038/nmeth.2967.

43. Zolotukhin, S., and Vandenberghe, L.H. (2022). AAV capsid design: a Goldilocks challenge. Trends Mol. Med. *28*, 183–193. https://doi.org/10.1016/j.molmed.2022.01.003.

44. Zhu, D., Rostami, M.R., Zuo, W.L., Leopold, P.L., and Crystal, R.G. (2020). Single-cell transcriptome analysis of mouse liver cell-specific tropism and transcriptional dysregulation following intravenous administration of AAVrh.10 vectors. Hum. Gene Ther. *31*, 590–604. https://doi.org/10.1089/hum.2019.366.

45. Öztürk, B.E., Johnson, M.E., Kleyman, M., Turunç, S., He, J., Jabalameli, S., Xi, Z., Visel, M., Dufour, V.L., Iwabe, S., et al. (2021). scAAVengr, a transcriptome-based pipeline for quantitative ranking of engineered AAVs with single-cell resolution. Elife *10*, e64175. https://doi.org/10.7554/eLife.64175.

46. Brown, D., Altermatt, M., Dobreva, T., Chen, S., Wang, A., Thomson, M., and Gradinaru, V. (2021). Deep parallel characterization of AAV tropism and AAV-mediated transcriptional changes via single-cell RNA sequencing. Front. Immunol. *12*, 730825. https://doi.org/10.3389/fimmu.2021.730825.

47. Lubelsky, Y., and Ulitsky, I. (2018). Sequences enriched in Alu repeats drive nuclear localization of long RNAs in human cells. Nature *555*, 107–111. https://doi.org/10.1038/nature25757.

48. Cunningham, S.C., Dane, A.P., Spinoulas, A., Alexander, I.E., and Alexander, I.E. (2008). Gene delivery to the juvenile mouse liver using AAV2/8 vectors. Mol. Ther. *16*, 1081–1088. https://doi.org/10.1038/mt.2008.72.

49. Bell, P., Wang, L., Gao, G., Haskins, M.E., Tarantal, A.F., McCarter, R.J., Zhu, Y., Yu, H., and Wilson, J.M. (2011). Inverse zonation of hepatocyte transduction with AAV vectors between mice and non-human primates. Mol. Genet. Metab. *104*, 395–403. https://doi.org/10.1016/j.ymgme.2011.06.002.

50. Fong, S., Yates, B., Sihn, C.R., Mattis, A.N., Mitchell, N., Liu, S., Russell, C.B., Kim, B., Lawal, A., Rangarajan, S., et al. (2022). Interindividual variability in transgene mRNA and protein production following adeno-associated virus gene therapy for hemophilia A. Nat. Med. *28*, 789–797. https://doi.org/10.1038/s41591-022-01751-0.

51. Lichter-Konecki, U., Caldovic, L., Morizono, H., Simpson, K., Ah Mew, N., and MacLeod, E. (1993). Ornithine transcarbamylase deficiency, M.P. Adam, G.M. Mirzaa, R.A. Pagon, S.E. Wallace, L.J.H. Bean, K.W. Gripp, and A. Amemiya, eds. (GeneReviews((R))).

52. Michailidis, E., Vercauteren, K., Mancio-Silva, L., Andrus, L., Jahan, C., Ricardo-Lax, I., Zou, C., Kabbani, M., Park, P., Quirk, C., et al. (2020). Expansion, in vivo-ex vivo cycling, and genetic manipulation of primary human hepatocytes. Proc. Natl. Acad. Sci. USA *117*, 1678–1688. https://doi.org/10.1073/pnas.1919035117.

53. Hao, Y., Hao, S., Andersen-Nissen, E., Mauck, W.M., 3rd, Zheng, S., Butler, A., Lee, M.J., Wilk, A.J., Darby, C., Zager, M., et al. (2021). Integrated analysis of multimodal single-cell data. Cell *184*, 3573–3587.e29. https://doi.org/10.1016/j.cell.2021.04.048.

54. Xiao, X., Li, J., and Samulski, R.J. (1998). Production of high-titer recombinant adeno-associated virus vectors in the absence of helper adenovirus. J. Virol. *72*, 2224–2232.

55. Khan, I.F., Hirata, R.K., and Russell, D.W. (2011). AAV-mediated gene targeting methods for human cells. Nat. Protoc. *6*, 482–501. https://doi.org/10.1038/nprot.2011.301.

56. Dane, A.P., Cunningham, S.C., Graf, N.S., and Alexander, I.E. (2009). Sexually dimorphic patterns of episomal rAAV genome persistence in the adult mouse liver and correlation with hepatocellular proliferation. Mol. Ther. *17*, 1548–1554. https://doi.org/10.1038/mt.2009.139.